Systematically smaller single-epoch quasar black hole masses using a radius–luminosity relationship corrected for spectral bias

Jaya Maithil [1]★ Michael S. Brotherton,[1] Ohad Shemmer,[2] Pu Du,[3] Jian-Min Wang,[3,4,5]
Adam D. Myers,[1] Jacob N. McLane,[1] Cooper Dix[2] and Brandon M. Matthews[2]

[1]*Department of Physics and Astronomy, University of Wyoming, Laramie, WY 82071, USA*
[2]*Department of Physics, University of North Texas, Denton, TX 76203, USA*
[3]*Key Laboratory for Particle Astrophysics, Institute of High Energy Physics, Chinese Academy of Sciences, 19B Yuquan Road, Beijing 100049, People's Republic of China*
[4]*National Astronomical Observatories of China, Chinese Academy of Sciences, 20A Datun Road, Beijing 100020, People's Republic of China*
[5]*School of Astronomy and Space Science, University of Chinese Academy of Sciences, 19A Yuquan Road, Beijing 100049, People's Republic of China*

ABSTRACT

Determining black hole masses and accretion rates with better accuracy and precision is crucial for understanding quasars as a population. These are fundamental physical properties that underpin models of active galactic nuclei. A primary technique to measure the black hole mass employs the reverberation mapping of low-redshift quasars, which is then extended via the radius–luminosity relationship for the broad-line region to estimate masses based on single-epoch spectra. An updated radius–luminosity relationship incorporates the flux ratio of optical Fe II to Hβ ($\equiv \mathcal{R}_{\mathrm{Fe}}$) to correct for a bias in which more highly accreting systems have smaller line-emitting regions than previously realized. In this work, we demonstrate and quantify the effect of using this Fe-corrected radius-luminosity relationship on mass estimation by employing archival data sets possessing rest-frame optical spectra over a wide range of redshifts. We find that failure to use an Fe-corrected radius predictor results in overestimated single-epoch black hole masses for the most highly accreting quasars. Their accretion rate measures ($L_{\mathrm{Bol}}/L_{\mathrm{Edd}}$ and $\mathscr{\dot{M}}$) are similarly underestimated. The strongest Fe-emitting quasars belong to two classes: high-z quasars with rest-frame optical spectra, which, given their extremely high luminosities, require high accretion rates, and their low-z analogues, which, given their low black holes masses, must have high accretion rates to meet survey flux limits. These classes have mass corrections downward of about a factor of two, on average. These results strengthen the association of the dominant Eigenvector 1 parameter $\mathcal{R}_{\mathrm{Fe}}$ with the accretion process.

Key words: galaxies: active – quasars: supermassive black holes.

1 INTRODUCTION

Black hole mass and accretion rate are arguably the two most important properties of quasars. They are vital in understanding the growth of supermassive black holes and how feedback from quasars regulates the growth of massive galaxies. In the past decade, more than 50 quasars have been discovered at $z > 6$ that are claimed to have billion solar mass black holes (e.g. Mortlock et al. 2011; Wang et al. 2021). Such findings challenge our understanding of black hole formation and growth. To form a billion solar mass black hole when the Universe was ≤ 1 Gyr old requires a massive seed black hole, $M_{\mathrm{seed}} \geq 10^{3} M_{\odot}$, in an Eddington-limited accretion rate scenario (e.g. Lodato & Natarajan 2006; Johnson et al. 2012). Alternatively, accretion with reduced radiative efficiency, $\epsilon = 0.01 - 0.001$, could explain the growth in such a short cosmic time (e.g. Volonteri, Silk & Dubus 2015; Trakhtenbrot, Volonteri & Natarajan 2017; Davies, Hennawi & Eilers 2019). Another possible explanation for such

apparently large quasar black hole masses at such early times could also simply be a systematic overestimation.

For nearby (distance <300 Mpc, $z < 0.06$) active galactic nuclei (AGNs), direct measurement of black hole mass is made using stellar and gas dynamics (Kormendy & Ho 2013). These methods are not possible for distant objects because of limited angular resolution and the fact that quasars outshine their host galaxy. Observations of the correlated variation of the continuum and photoionized broad emission lines (especially Balmer lines) in type-1 AGNs led to the development of the reverberation mapping (RM) technique to determine black hole masses (e.g. Peterson 1993). Time delays between the continuum and emission-line variability, derived from multiple epochs of spectroscopy, can be used to measure the size of the broad-line region (BLR) (Blandford & McKee 1982; Netzer & Peterson 1997; Peterson 1993, 2014). Combining this measurement with the emission-line velocity dispersion provides an estimate of the virialized black hole mass (see equation 1) (Peterson et al. 2004). Over the past two decades, RM has provided black hole mass measurements for over a hundred AGNs (e.g. Bentz & Katz 2015; Yu et al. 2020a). However, it is impractical to apply the RM method for

★ E-mail: jaya.maithil1109@gmail.com

every AGN as it is resource-intensive. Fortunately, RM studies show a relationship between the BLR size and the continuum luminosity to be R ∝ $L^{\sim 0.5}$ (Kaspi et al. 2000, 2005, 2007, 2021; Bentz et al. 2006, 2009, 2013). RM studies based on the Hβ line provide the most reliable correlations (Bentz et al. 2013). Using the luminosity at 5100Å from single-epoch (SE) spectra, one can then predict the size of the BLR and estimate the black hole mass (e.g. Laor 1998; Wandel, Peterson & Malkan 1999; Vestergaard & Peterson 2006).

For the highest redshift quasars, most of the optical-UV lines fall in the near-infrared part of the spectrum, for which there are fewer spectral observations. The masses of the black holes that power high-redshift quasars are therefore estimated using UV continuum luminosities and emission lines like C IV and Mg II, calibrated against Hβ RM measurements, a procedure that introduces additional uncertainties. The offset between Mg II- or C IV-based black hole masses with Hβ-based masses is in part related to Eigenvector 1 (EV1) spectral trends (e.g. Shen et al. 2008; Runnoe et al. 2013b; Brotherton et al. 2015) that appear to be correlated with Eddington ratio (Boroson & Green 1992; Marziani et al. 2001; Boroson 2002; Yuan & Wills 2003; Shen & Ho 2014; Sun & Shen 2015). Shen et al. (2008) demonstrated that the offset between Mg II- and C IV-based SE black hole mass correlates with another EV1 parameter, C IV blueshift. Runnoe et al. (2013b) identified a similar bias in C IV-based masses using the ratio of C IV to the λ1400 feature (a blend of Si IV + O IV]). Brotherton et al. (2015) demonstrated that an EV1 bias in reverberation-mapped AGN samples leads to a 50 per cent overestimation of C IV-based masses in average quasars. Recent results from Dalla Bontà et al. (2020) show that the difference between C IV-based RM masses and SE masses anticorrelates with Eddington ratio.

The Hβ RM sample originally used to establish the R-L relationship primarily included objects with strong narrow [O III] emission lines. This is because [O III] lines are convenient for relative flux calibration (van Groningen & Wanders 1992) and such objects also tend to have strong broad Hβ line variability. The equivalent width (EW) of [O III] is anticorrelated with the Eddington ratio (L_{bol}/L_{Edd}, described in Section 2) (Boroson & Green 1992; Marziani et al. 2001; Boroson 2002; Shen & Ho 2014), hence, RM samples were biased towards low-accretion-rate broad-lined AGNs (i.e. Eddington ratio of a few to a few tens of per cent). Recent Hβ RM campaigns, such as the Super-Eddington Accreting Massive Black Hole (SEAMBH; Du et al. 2014, 2016, 2018) and the Sloan Digital Sky Survey Reverberation Mapping projects (SDSS-RM; Shen et al. 2015) find deviations from the canonical R-L relationship. The observed time lags are sometimes significantly smaller than predicted (Du et al. 2015, 2016, 2018; Grier et al. 2017; Du & Wang 2019). The offsets in the Hβ SDSS-RM sample are not due to observational bias, but rather they reflect the wide variety of broad-line radii occupied by AGNs (Fonseca Alvarez et al. 2020). Moreover, the offset between the observed and predicted BLR radius shows an anticorrelation with the EV1 accretion rate parameters (Du et al. 2018; Du & Wang 2019; Dalla Bontà et al. 2020). Even the Mg II and C IV RM samples demonstrate similar offsets in BLR radius that are correlated with accretion rate parameters, suggesting that current R-L relationships should include some additional correction terms (Dalla Bontà et al. 2020; Martínez-Aldama et al. 2020).

The SEAMBH Hβ RM sample comprises a population of highly accreting AGNs with a BLR radius up to three to eight times smaller than predicted from the canonical R-L relationship, which implies an overestimation of SE black hole masses by the same factor. The SEAMBH RM results also establish a strong anticorrelation between the deviation from the canonical R-L relationship and the

relative strength of Fe II, an EV1 parameter that correlates with the Eddington ratio. Using a sample of 75 RM AGNs, Du & Wang (2019) updated and tightened the R-L relationship by introducing the relative strength of Fe II as a predictive parameter. Yu et al. (2020a) provide a similar accretion-rate-based correction to the R-L relation using the strength of Fe II. Such a correction should be extremely significant for luminous high-redshift quasars, which are likely to be accreting at a high rate. Using the Eddington ratio distribution for a uniformly selected sample of type 1 quasars from SDSS DR7, Kelly & Shen (2013) employed a flexible Bayesian technique to demonstrate that the fraction of quasars with a higher Eddington ratio becomes larger at high redshift. Therefore, the canonical R-L relationship most likely overestimates the masses of the black holes hosted by high-redshift quasars. Similarly, the dimensionless accretion rate parameter ($\mathscr{\dot{M}}$) and Eddington ratio, which are inversely proportional to black hole mass, are likely to be underestimated. Even this underestimated $\mathscr{\dot{M}}$ results in a large population of super-Eddington quasars, $\mathscr{\dot{M}} > 3$, which necessitates the use of an accretion-rate-corrected R-L relationship (see figure comparing canonical and Fe-corrected accretion rate parameter in Section 4).

This paper adopts the Du & Wang (2019) R-L relationship to quantify this effect using archival data of low- and high-redshift quasars. Our results demonstrate that for objects with large $\mathcal{R}_{Fe}$, the SE method adopting the canonical R-L relation significantly overestimates their Hβ-based masses and underestimates their accretion rates by factors of a couple to several. In Section 2, we explain the method to determine black hole mass and accretion rate parameters with the new and canonical R-L relationship. Section 3 describes the low- and high-redshift samples used and summarizes the quantities used to estimate black hole mass. We discuss our results regarding the black hole mass and accretion rate in Section 4.1 and the correlation between $\mathcal{R}_{Fe}$ and accretion rate parameters in Section 4.2, followed by additional discussion and conclusions in Sections 5 and 6, respectively. Throughout the paper, we adopt a cosmology with $H_0 = 70$ km s^{-1} Mpc^{-1}, $\Omega_\Lambda = 0.7$, and $\Omega_m = 0.3$.

2 BLACK HOLE MASS AND ACCRETION RATE

Black hole masses (M_{BH}) are estimated using the following relationship:

$$M_{BH} = f\left(\frac{R_{BLR}\Delta V^2}{G}\right).\tag{1}$$

This equation assumes the virialized motion of BLR clouds under the gravitational potential of the central black hole (e.g. Wandel et al. 1999; Peterson et al. 2004). The expression in parenthesis is called virial product. The full width at half-maximum (FWHM) or line dispersion (σ_{line}) of broad emission lines like Hβ sets the velocity (ΔV) assuming Doppler broadening. The size of the BLR, R_{BLR}, can then be determined by multiplying the time lag ($\Delta\tau$) between emission-line and continuum variability, determined by RM, by the speed of light ($R_{BLR} = c\Delta\tau$). The virial coefficient, f, accounts for the unknown geometry, kinematics, and inclination of the BLR. Although its value differs from one AGN to another, a mean value of f is obtained empirically by calibrating RM mass against mass predicted by the M–$\sigma_\star$ relation seen in quiescent galaxies (Onken et al. 2004, and many others since). Here, we focus on Hβ-based SE virial black hole mass and adopt FWHM of Hβ as the measure of ΔV.

The monochromatic luminosity at 5100Å in erg s^{-1}, $\lambda L_{\lambda, 5100Å}$ (hereafter $L_{5100Å}$), serves as a proxy for R_{BLR}. We use two R-L

relationships: (1) the canonical R-L relationship established by Bentz et al. (2013)

$$\log (R_{H\beta}/\text{lt} - \text{days}) = K + \mu \log (L_{5100\text{Å}}/10^{44} \text{ erg s}^{-1}), \qquad (2)$$

where, $K = 1.527 \pm 0.031$ and $\mu = 0.533 \pm 0.035$, and (2) an accretion-rate-corrected R-L relationship established by Du & Wang (2019)

$$\log (R_{H\beta}/\text{lt} - \text{days}) = \alpha + \beta \log \ell_{44} + \gamma \mathcal{R}_{\text{Fe}}, \qquad (3)$$

where, $\ell_{44} = L_{5100\text{Å}}/10^{44}$ erg s^{-1}, $\alpha = 1.65 \pm 0.06$; $\beta = 0.45 \pm 0.03$; $\gamma = -0.35 \pm 0.08$. It takes into account the relative strength of Fe II, $\mathcal{R}_{\text{Fe}}$, that is known to correlate with EV1. $\mathcal{R}_{\text{Fe}}$ is defined as the ratio of flux (F) or rest-frame EW between Fe II and Hβ, i.e. $\mathcal{R}_{\text{Fe}} = F(\text{Fe II})/F(H\beta) \approx \text{EW(Fe II)/EW(H}\beta)$. A higher $\mathcal{R}_{\text{Fe}}$ value leads to a systematically smaller R_{BLR} estimate and is likely associated with a higher accretion rate (Du & Wang 2019, and our discussion later in this paper).

We estimate the SE virial black hole mass by determining R_{BLR} from the R-L relationships, using FWHM of Hβ as the velocity term, and a virial coefficient $f = 1.5$ in equation (1). Our choice of the virial coefficient is consistent with the empirical mean value of f obtained by calibrating FWHM-based RM black hole mass from rms spectra with the M–$\sigma_\star$ relation. We adopted the Ho & Kim (2014) value of $f = 1.5 \pm 0.4$ for AGNs in classical bulges and ellipticals that have black hole mass greater than $10^7 M_\odot$. Recent work by Yu et al. (2019, 2020b) also finds $f = 1.51 \pm 0.20$ for low-redshift RM AGNs in classical bulges and ellipticals. Henceforth, we shall refer to the SE black hole mass estimated using equation (2) as the 'canonical' black hole mass, $M_{H\beta, \text{canonical}}$ and the one using equation (3) as the 'Fe-corrected' black hole mass, $M_{H\beta, \text{Fe-corrected}}$. Note that we adopt $f = 1.5$ for both canonical and Fe-corrected black hole mass estimates. Therefore, the $\mathcal{R}_{\text{Fe}}$ factor in the Du & Wang (2019) R-L relationship (equation 3) dominates the difference between $M_{H\beta, \text{canonical}}$ and $M_{H\beta, \text{Fe-corrected}}$.

We calculate two relative accretion rate parameters based on luminosity and black hole mass. First, there is the dimensionless accretion rate parameter, $\dot{\mathcal{M}}$, derived from the Shakura & Sunyaev (1973) thin accretion disc model for which

$$\dot{\mathcal{M}} = 20.1 (\ell_{44}/\cos i)^{3/2} m_7^{-2}, \qquad (4)$$

where $m_7 = M_{\text{BH}}/10^7 M_\odot$ and i is inclination angle to the line of sight (Du et al. 2014, 2018; Wang et al. 2014b; Du & Wang 2019). We take $\cos i = 0.75$, an average for type 1 AGNs, for our calculation. Second, we have the Eddington ratio, ($L_{\text{bol}}/L_{\text{Edd}}$) expressed as the ratio of the bolometric luminosity (L_{Bol}) to the Eddington luminosity ($L_{\text{Edd}} = 1.5 \times 10^{45} m_7$ erg s^{-1}). We calculate L_{Bol} using the Richards et al. (2006) relation, $L_{\text{Bol}} = 9.26 L_{5100\text{Å}}$.

$$\frac{L_{\text{bol}}/L_{\text{Edd}}}{1.5 \times 10^{45} m_7} = \frac{9.26 L_{5100\text{Å}}}{1.5 \times 10^{45} m_7} \qquad (5)$$

The bolometric luminosity may saturate in the case of quasars with super-Eddington accretion owing to the photon trapping effect in their slim accretion discs (Wang et al. 1999; Mineshige et al. 2000). This, in principle, may make $\dot{\mathcal{M}}$ a better predictor of accretion rate, although the two are highly correlated for quasars, as we will show.

For the flux-to-luminosity conversion we use $\lambda L_\lambda [\text{erg s}^{-1}] = 4\pi D_L^2 f_\lambda (1 + z) \lambda$, where f_λ is the monochromatic flux at the rest-wavelength (λ) in units of erg s^{-1} cm^{-2} Å^{-1}, D_L is the luminosity distance, and z is the redshift (Hogg et al. 2002).

3 ARCHIVAL DATA SETS AND MEASUREMENTS

To characterize the effect of using the new R-L relationship (equation 3) on Hβ-based black hole mass estimates, and hence also estimates of accretion rate, we selected archival samples and associated catalogues that provide: (a) flux or EW of Fe II between rest-frame 4435–4685 Å and the broad Hβ component to calculate $\mathcal{R}_{\text{Fe}}$, (b) flux or luminosity at rest-frame 5100 Å to estimate the BLR size from the new R-L relationship, and (c) FWHM Hβ to provide a proxy for velocity dispersion.

For low-redshift quasars ($z < 0.7$), we used only the catalogue of Shen et al. (2011), which is highly complete with uniform measurements of the quantities we need for objects in the Sloan Digital Sky Survey Data Release 7 (SDSS DR7 Abazajian et al. 2009). The Shen et al. (2011) catalogue contains a total of 105 783 quasars. We applied a conservative signal-to-noise ratio (S/N) and redshift cut-off to obtain a sample unbiased by poor-quality spectra in the Hβ region. Our selection criteria include a median S/N per pixel in the Hβ region greater than 20, redshift $z < 0.7$, and non-zero measurements of EW and FWHM Hβ. Our choice of S/N > 20 per pixel eliminates unreliable line width measurements and reduces the formal uncertainties in SE masses to a minimum (Denney et al. 2009). Given the automatic nature of spectral fits in Shen et al. (2011), some individual measurements are bad. So we applied a S/N > 3 cut on the Hβ line measurements as an additional quality control check. We eliminated three targets, SDSS J094927.67+314110.0, SDSS J105528.80+312411.3, and SDSS J151036.74+510854.6 because of erroneous measurements due to incorrect redshifts,[1] giving a total of 3309 quasars.

Shen et al. (2011) did not correct the catalogued 5100 Å luminosities for host-galaxy contamination. We applied a correction when $\log[L_{5100\text{Å}}/(\text{erg s}^{-1})] < 45.053$, using equation (1) of Shen et al. (2011). Recently, Dalla Bontà et al. (2020) defined a host-galaxy light correction based on the luminosity of the Hβ line, L(Hβ). We tested the effect of our choice of using Shen et al. (2011) host-galaxy correction method against the method described by Dalla Bontà et al. (2020) for the canonical and Fe-corrected black hole mass estimates. There is essentially no change in the mass difference distribution between the two different methods when correcting $L_{5100\text{Å}}$ for the low-luminosity subsample ($\log [L_{5100\text{Å}}/(\text{erg s}^{-1})] < 45.0$). The mean mass differences are 0.14 dex with the Shen et al. correction, 0.13 dex with the Dalla Bontà et al. correction, and the standard deviations are 0.19 and 0.18 dex, respectively. There are systematic differences in the host-galaxy correction method defined by Dalla Bontà et al. and Shen et al.. On average, Dalla Bontà et al. method underestimates $L_{5100\text{Å}}$ by a factor of 1.28 compared to Shen et al. method. For highly luminous quasars ($\log [L_{5100\text{Å}}/(\text{erg s}^{-1})] > 45.0$), the mean underestimation in $L_{5100\text{Å}}$ by Dalla Bontà et al. method is a factor of 1.32 compared to Shen et al., with 40 per cent of quasars underestimated by a factor of 1.32–13.18. Note that the Shen et al. method is not sensitive to any host galaxy emission when the spectral absorption features disappear; hence this method underestimates the host-galaxy correction for the most luminous quasars. Even though the Dalla Bontà et al. L(Hβ)–$L_{5100\text{Å}}$ correlation is relatively tight, it is based on a small sample, and there may be issues extrapolating to higher $L_{5100\text{Å}}$. There is an additional concern that EW Hβ correlates with $\mathcal{R}_{\text{Fe}}$ ($P < 1$ per cent; Boroson & Green

---

[1]While inspecting the SDSS spectrum of outliers in Figs 7, 8, and 9, these three quasars had wrong redshifts assigned to them.
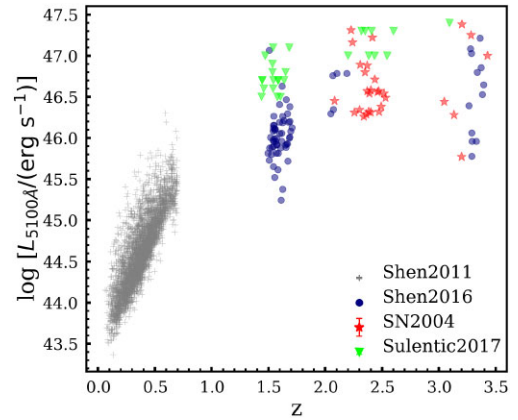
Table 1. Data sets used in our analysis.

Ref	Sample	Sample size	Redshift
Shen et al. (2011)	Shen2011	3309	<0.7
Shen (2016)	Shen2016	71	1.5–3.5
Shemmer et al. (2004)	SN2004	29	2–3.5
Netzer et al. (2004)			
Sulentic et al. (2017)	Sulentic2017	26	1.4–3.1

1992) and using an $L_{5100\text{Å}}$ based on $L(\text{H}\beta)$ might bias Fe-corrected black hole mass estimates.

For high-redshift quasars, the H β region falls in the near-infrared (IR). A good S/N near-IR spectrum of a low-luminosity high-redshift quasar requires an exorbitantly large amount of observing time on most telescopes. As a result, archival samples at high redshift predominantly contain high-luminosity quasars. Only a handful of samples tabulate the Fe II measurement essential for our study. Our analysis includes all the high-redshift samples we found that provide good spectral measurements required to calculate canonical and Fe-corrected black hole mass. These high-redshift samples are a near-IR follow-up of quasars with previous rest-frame UV spectral observation selecting targets based primarily on two criteria: (1) high S/N ratio in the spectral region containing UV emission lines like C IV and N V and (2) redshifts for which H β falls in unobscured near-IR spectral bands (i.e. JHK bands). Appendix A provides more detailed information about the individual sample selection of the high-redshift samples from the work of Shen (2016), the two-part series by Shemmer et al. (2004) & Netzer et al. (2004) (hereafter SN2004), and Sulentic et al. (2017).

Table 1 lists the name of the samples we use, their total number of objects, and their redshift range. Shen (2016) contains 74 quasars in the redshift range $1.5 \leq z \leq 3.5$. We eliminated one quasar, J0810+0936, with a strangely large uncertainty reported for its luminosity measurement ($\log [L_{5100\text{Å}}/(\text{erg s}^{-1})] = 46.30 \pm 23.16$). Shen (2016) reports rest-frame EWs, which we used to calculate $\mathcal{R}_{\text{Fe}}$, and include 71 quasars with $\mathcal{R}_{\text{Fe}} < 3$. SN2004 consists of 29 quasars in the redshift range $2 \leq z \leq 3.5$. We used the tabulated systemic redshift, 5100Å luminosity, and the best-fitting FWHM H β values from Shemmer et al. (2004), and $\mathcal{R}_{\text{Fe}}$ measurements given by Netzer et al. (2004). Sulentic et al. (2017) catalogue the properties of a sample of 28 quasars with $1.4 \leq z \leq 3.1$, including two weak-line quasars (HE0359-3959, HE2352-4010) that we eliminate for our analysis.[2] We used their tabulated $\mathcal{R}_{\text{Fe}}$ measurements and FWHM H β of the broad component obtained from the spectral fit analysis. Our final combined sample provides redshift coverage $0.05 < z < 3.6$ and represents a typical range of luminosity seen in low- and high-redshift quasars (Fig. 1).

We calculated $M_{\text{H}\beta,\,\text{canonical}}$ for all samples using the canonical R-L relation (equation 2), with FWHM H β as a proxy for the velocity, and $f = 1.5$ in equation (1). All of these literature sources except Sulentic et al. (2017) provide EWs, and use the EW ratio as $\mathcal{R}_{\text{Fe}}$. Netzer et al. (2004) mention that the flux ratio is the same as the EW ratio used to define $\mathcal{R}_{\text{Fe}}$ by Boroson & Green (1992). Sulentic et al. (2017) use line flux ratios to calculate $\mathcal{R}_{\text{Fe}}$, and note that this is equivalent to using EW ratios. We used the Du & Wang (2019) R-L relation (equation 3), with FWHM H β as a proxy for the velocity and $f = 1.5$ in equation (1), to calculate $M_{\text{H}\beta,\,\text{Fe-corrected}}$ for each sample. For Shen et al. (2011) quasars, we used the luminosity

---

[2]We include the two weak-line quasars from Sulentic et al. (2017) and two others from Shemmer et al. (2010) in Appendix B

Figure 1. Redshift versus $\log L_{5100\text{Å}}$. The plot shows the redshift–luminosity space spanned by our quasar samples.

corrected for host-galaxy contamination to estimate both $M_{\text{H}\beta,\,\text{canonical}}$ and $M_{\text{H}\beta,\,\text{Fe-corrected}}$.

For Shen et al. (2011) and Shen (2016) samples, we propagated the measurement uncertainties in FWHM H β, $L_{5100\text{Å}}$, EW H β, and EW Fe II to calculate the error in the derived quantities like $\mathcal{R}_{\text{Fe}}$, R_{BLR}, M_{BH}, $L_{\text{Bol}}/L_{\text{Edd}}$, and $\dot{\mathcal{M}}$. For other samples, we made a few assumptions to estimate measurement uncertainties. SN2004 provide the uncertainty in FWHM H β as the difference between direct and best-fitting measures for each source and quotes an average uncertainty of 25 per cent on $L_{5100\text{Å}}$. We assumed an uncertainty of 24 per cent for $\mathcal{R}_{\text{Fe}}$ based on the mean uncertainty reported by McIntosh et al. (1999) with similar data quality and spectral resolution. Sulentic et al. (2017) list uncertainty in 5100Å flux but do not provide uncertainties in spectral measurements. Sulentic et al. (2017) obtained the spectra from the parent samples of Sulentic et al. (2004, 2006) and Marziani et al. (2009) and redid the analysis; their spectral measurements are consistent but not identical. So we obtained the relative error in FWHM H β, EW H β, and EW Fe II for each target in Sulentic et al. (2017) from the parent samples to estimate uncertainties in derived quantities. Our error propagation also includes uncertainties in the virial coefficient (f) and the coefficients in the two R-L relationships. We list the mean measurement uncertainties in the derived quantities for each sample in Table 2 and show them as typical error bars in our figures.

4 RESULTS

Fig. 2 shows the Fe-corrected R-L relationship (equation 3) for all the samples. For the luminous high-z quasars with strong $\mathcal{R}_{\text{Fe}}$, the Du & Wang (2019) R-L relation gives a smaller R_{BLR} as compared to the canonical R-L relationship (equation 2). The same effect emerges in low-z quasars with strong $\mathcal{R}_{\text{Fe}}$. For low-z quasars with $0 \leq \mathcal{R}_{\text{Fe}} \leq 0.42$, the $\mathcal{R}_{\text{Fe}}$ correction is small, and the Du & Wang (2019) R-L relation gives a larger R_{BLR} owing to the difference in zero-point and coefficient of luminosity ($\alpha = 1.65$, $\beta = 0.45$) compared to the canonical R-L relationship ($K = 1.527$, $\mu = 0.533$). These differences in the predicted R_{BLR} from the two R-L relationships propagate to their black hole mass estimates and consequently to the accretion rates.
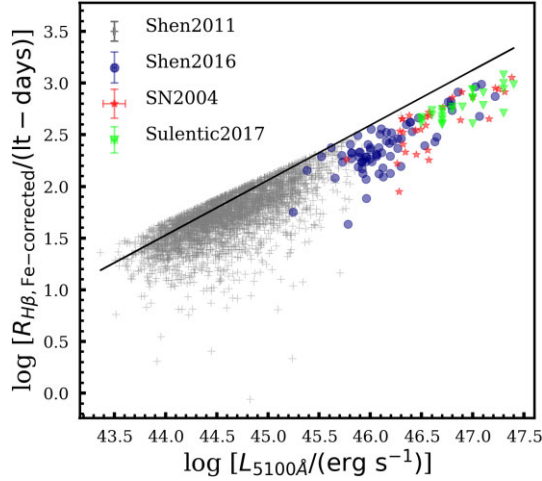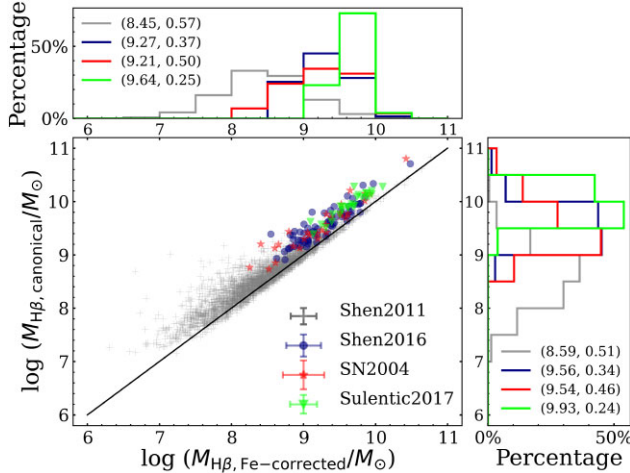
4.1 The effects of the Fe correction on mass and accretion rate

Fig. 3 compares the Fe-corrected black hole masses against the canonical masses. The majority of the points (80 per cent) lie above

Table 2. Mean measurement uncertainties on the derived quantities for each sample.

Quantities	Mean measurement error			
	Shen2011	Shen2016	SN2004	Sulentic2017
$R_{\mathrm{H}\beta,\,\mathrm{canonical}}$	0.04 dex	0.08 dex	0.11 dex	0.11 dex
$M_{\mathrm{H}\beta,\,\mathrm{canonical}}$	0.15 dex	0.20 dex	0.27 dex	0.17 dex
$L_{\mathrm{Bol}}/L_{\mathrm{Edd},\,\mathrm{canonical}}$	0.15 dex	0.20 dex	0.27 dex	0.17 dex
$\mathcal{M}_{\mathrm{canonical}}$	0.30 dex	0.41 dex	0.53 dex	0.35 dex
$\mathcal{R}_{\mathrm{Fe}}$	0.10 dex	0.15 dex	0.10 dex	0.11 dex
$R_{\mathrm{H}\beta,\,\mathrm{Fe\text{-}corrected}}$	0.10 dex	0.15 dex	0.14 dex	0.13 dex
$M_{\mathrm{H}\beta,\,\mathrm{Fe\text{-}corrected}}$	0.17 dex	0.24 dex	0.29 dex	0.19 dex
$L_{\mathrm{Bol}}/L_{\mathrm{Edd},\,\mathrm{Fe\text{-}corrected}}$	0.18 dex	0.24 dex	0.29 dex	0.19 dex
$\mathcal{M}_{\mathrm{Fe\text{-}corrected}}$	0.35 dex	0.48 dex	0.57 dex	0.37 dex

Figure 2. Fe-corrected R_{BLR} using equation (3) versus 5100Å luminosity for our quasar samples. The black solid line represents the canonical R-L relation. It shows that the Du & Wang (2019) R-L relation predicts a smaller BLR radius than the canonical R-L relation for higher accretion rate quasars marked with strong $\mathcal{R}_{\mathrm{Fe}}$.

Figure 3. Black hole mass calculated using the canonical (*y*-axis) and Fe-corrected (*x*-axis) R-L relation. The histograms on top and right show the percentage distributions (i.e. the fraction of targets in each bin × 100) of the Fe-corrected and canonical mass, respectively. The numbers in brackets give the mean and standard deviation of each sample. The plot shows that the black hole mass is systematically overestimated using the canonical R-L relation.

the 1:1 line, indicating a systematic overestimation of black hole mass when using the canonical R-L relation. Non-parametric tests such as Kolmogorov–Smirnov (K-S) test ($p = 1.84\mathrm{e}\text{-}22$) and the Wilcoxon rank sum test (two-sided $p = 6.27\mathrm{e}\text{-}25$) indicate that the differences in values and overall distributions between the two sets of masses significantly differ, as expected, since $\mathcal{R}_{\mathrm{Fe}}$ values are significantly above zero in significant fractions of the quasar population. It should be noted that the K-S and Wilcoxon rank sum tests do not take into account the measurement errors. We will discuss the $\mathcal{R}_{\mathrm{Fe}}$ distribution for our samples in Section 5.1.

The low-z Shen et al. (2011) quasars have a very large range in black hole masses, $10^6 < M_{\mathrm{BH}}(M_\odot) < 10^{11}$. The higher redshift samples have a smaller range of black hole masses, $10^8 < M_{\mathrm{BH}}(M_\odot) < 10^{10.5}$. Fig. 3 also shows that the deviation from the 1:1 line becomes pronounced moving to the very lowest mass quasars, $M_{\mathrm{BH}} < 10^8 M_\odot$. These low-mass quasars have larger $\mathcal{R}_{\mathrm{Fe}}$ and higher accretion rates (see figures showing the mass vs accretion rate plane and the distribution of $\mathcal{R}_{\mathrm{Fe}}$ in the Section 5.1) resulting in smaller Fe-corrected black hole masses. Therefore, in the low-z quasars, the Fe-correction is most important for the less massive, highly accreting objects. The subplots on the right and top show the percentage of the canonical and Fe-corrected mass, respectively, for each sample and their statistical means and standard deviations. The mean of each sample shifts to a lower M_{BH} when using the Du & Wang R-L relation. Note that Shen et al. (2011) sample consists of a tiny population (20 out of 3309) of quasars with $10^6 \leq M_{\mathrm{BH}}(M_\odot) \leq 10^7$ for which $f = 0.7 \pm 0.2$ may be more appropriate (Ho & Kim 2014, for the low-mass AGNs with pseudobulges). Our choice of $f = 1.5$ likely overestimates both the canonical and Fe-corrected black hole masses of these 20 quasars alike, although without impacting the ratio of the canonical to Fe-corrected mass.

To further illustrate the change in mass when the Fe correction is applied, we plot the distribution of the log of the ratio of canonical-to-Fe-corrected mass for the low-z Shen et al. (2011) sample in the left-hand and the middle panels of Fig. 4. The left histogram consists of quasars with $M_{\mathrm{Fe\text{-}corrected}} < 10^8 M_\odot$, whereas the middle panel shows quasars with $M_{\mathrm{Fe\text{-}corrected}} \geq 10^8 M_\odot$. The low-mass quasars ($<10^8 M_\odot$), on average, have a much larger overestimation, a factor of ~ 2, compared to a factor of ~ 1.3 for the high-mass ($\geq 10^8 M_\odot$) quasars in the low-z sample. The low-mass quasars are the ones with the strongest $\mathcal{R}_{\mathrm{Fe}}$ (see the $\mathcal{R}_{\mathrm{Fe}}$ distribution plot shown in the Section 5.1). For the low-z quasars with weaker $\mathcal{R}_{\mathrm{Fe}}$, using the Du & Wang (2019) R-L relation slightly overestimates the black hole mass of ~ 22 per cent of the sample compared to the canonical, owing to small differences in intercept and coefficient of luminosity.

The right histogram of Fig. 4 illustrates the change in mass for samples from Table 1, which excludes Shen et al. (2011). On average,
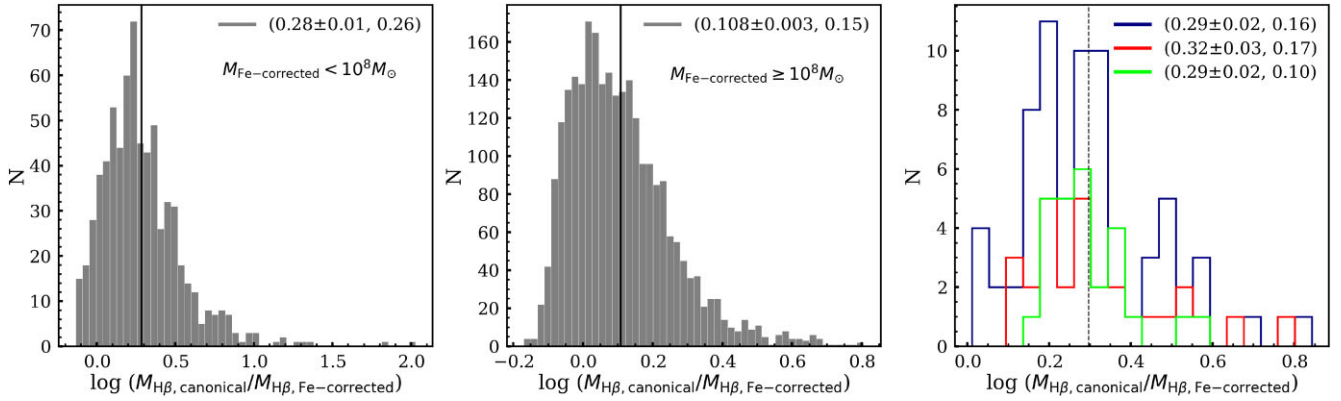
Figure 4. Left-hand panel: Histogram of the distribution of mass ratios for the low-z Shen2011 quasars with mass less than $10^8 M_\odot$. The mean $\pm$ the standard error of the mean, and the standard deviation for each sample are given in the parentheses. The mean ratio for this low-mass subsample is 0.28 ± 0.01, represented by the b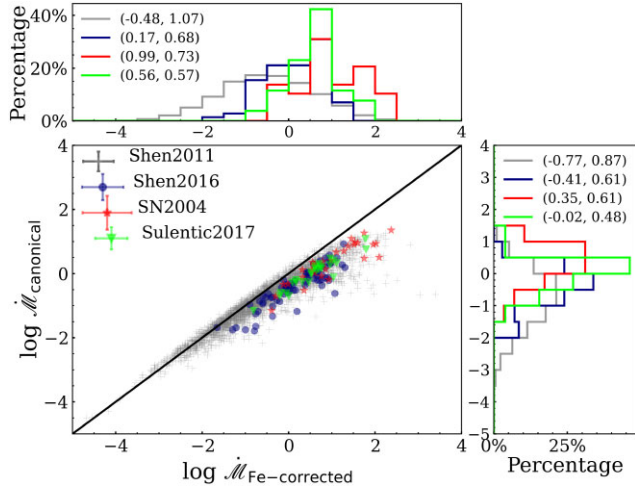lack solid line, and the standard deviation is 0.26, as stated in parentheses. Middle: Same as left figure but for the Shen2011 quasars with mass $\geq 10^8 M_\odot$. The mean ratio for the high-mass subsample is 0.108 ± 0.003, represented by the black solid line, and the standard deviation is 0.15, as given in parentheses. Right-hand panel: Histogram of the distribution of mass ratio for the high-z samples colour-coded for each sample same as Fig. 3. The individual mean and standard deviation are given in the parentheses. The mean ratio for the high-z samples is 0.30 ± 0.01, represented by the black dashed line, and the standard deviation is 0.18.

Figure 5. Canonical versus Fe-corrected accretion rate calculated using equation (3). It shows that the accretion rate is systematically underestimated when the canonical R-L relationship based black hole mass is used. The histograms on the right and top show the percentage distribution (i.e. the fraction of targets in each bin $\times$ 100) of canonical and Fe-corrected accretion rate, respectively. They show that the mean accretion rate for each sample increases when the Fe-corrected R-L relationship based mass is used.
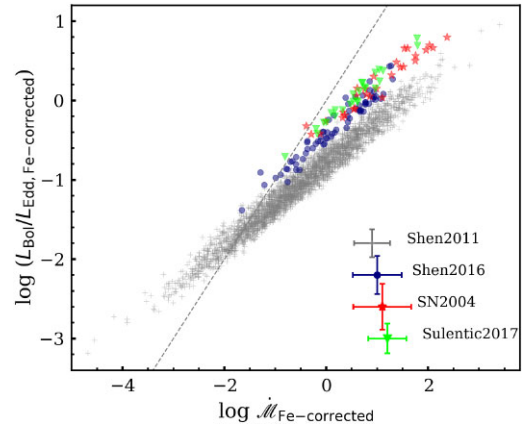

Figure 6. Corrected Eddington ratio versus accretion rate parameter for all samples. The grey dashed line represents the 1:1 relation for reference.

the black hole masses of these high-z samples decrease by about 0.3 dex or a factor of 2, as depicted by the dotted black line. The difference is up to a factor of 2 for 60 per cent of the sample and a factor of 2–4.7 for 37 per cent. The mean difference in mass in Shen (2016) is a factor of $\sim$2, in SN2004 is a factor of $\sim$2.1, and in Sulentic et al. (2017) is a factor of $\sim$2.

Next, we calculated the dimensionless accretion rate parameter defined in equation (4) using both canonical and Fe-corrected black hole mass. The comparison between canonical and Fe-corrected $\dot{\mathcal{M}}$ (Fig. 5) demonstrates that the accretion rates are underestimated, in agreement with the inverse relationship between $\dot{\mathcal{M}}$ and the black hole mass. The distribution in Fig. 5 shows that the mean $\dot{\mathcal{M}}$ for each sample is larger for the Fe-corrected black hole mass. For low-z quasars, i.e. the Shen et al. (2011) sample, the logarithm

of $\dot{\mathcal{M}}_{\text{Fe-corrected}}$ has a mean $\pm$ the standard error of the mean[3] of -0.48 ± 0.02, and it ranges from -4.68 to 3.40, although the high-z quasars (samples other than Shen et al. 2011) have systematically higher log $\dot{\mathcal{M}}_{\text{Fe-corrected}}$ values with a mean of 0.44 ± 0.07 and range from -1.66 to 2.37. Fig. 6 compares $\dot{\mathcal{M}}$ with the traditionally used Eddington ratio, both calculated using the Fe-corrected black hole mass. The log of the Fe-corrected Eddington ratio for the low-z quasars ranges from -3.19 to 0.95 and has a mean value of -1.04 ± 0.01, whereas the high-z quasars have a higher mean value of log $L_{\text{Bol}}/L_{\text{Edd, Fe-corrected}} = -0.13 \pm 0.04$ and range from -1.38 to 0.80.

As mentioned earlier, the canonical and Fe-corrected black hole mass differ primarily due to the $\mathcal{R}_{\text{Fe}}$ factor, an accretion rate indicator. Therefore, the plot of the change in the black hole mass or the mass ratio exhibits the expected strong correlation with the two accretion rate parameters, $L_{\text{Bol}}/L_{\text{Edd}}$ and $\dot{\mathcal{M}}$ (Fig. 7). We visually inspected the

---

[3]Note that the standard error of the mean quoted in the figures and text is purely statistical in nature (ratio of standard deviation and square root of sample size) and does not take into account the measurement uncertainties.
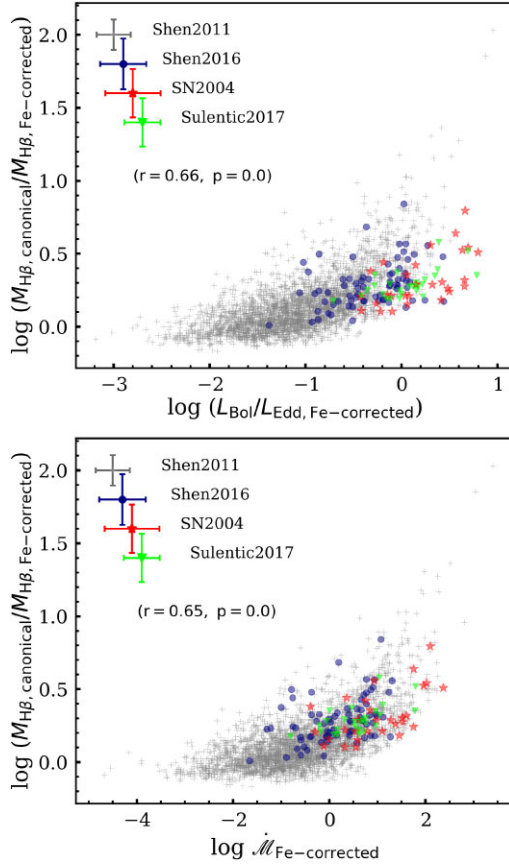
Figure 7. Mass ratio versus Fe-corrected Eddington ratio (top panel) and dimensionless accretion rate (bottom panel). Change in mass shows a strong correlation with the accretion rate parameters. The Pearson r coefficients for these correlations are given in parentheses.
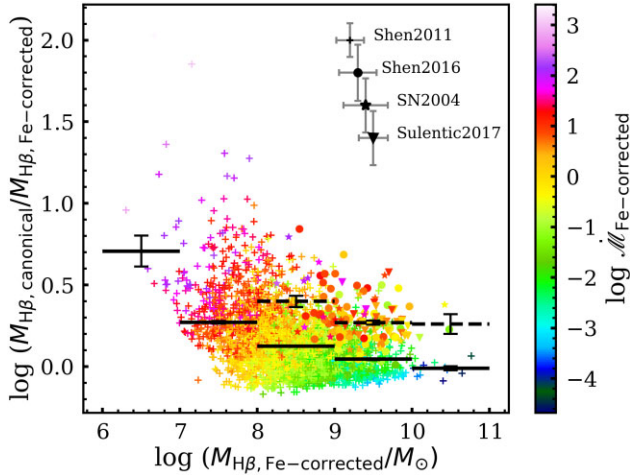

Figure 8. Mass ratio versus Fe-corrected black hole mass colour-coded by accretion rate. The black solid and dashed lines represent the mean mass ratio in each mass bin for the low-z sample and the high-z samples, respectively. The black error bars represent the standard error of the mean ratio in each mass bin. The grey error bars on the top of each sample represent the typical measurement error in the mass ratio. For $M_{H\beta, \text{Fe-corrected}} > 10^8 M_\odot$, the high-$z$ samples have a mean mass ratio greater than the low-z sample.
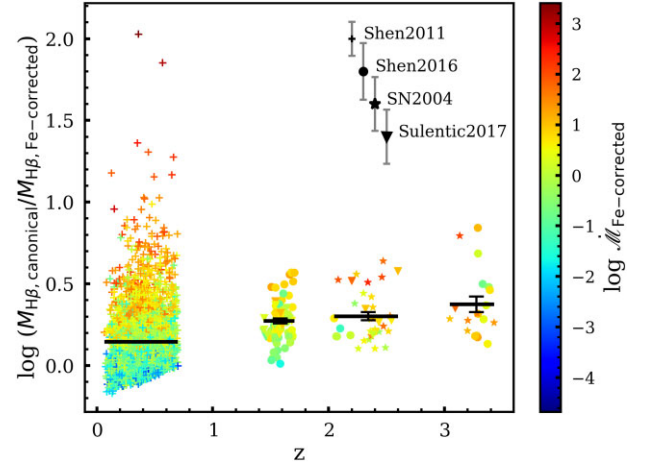

Figure 9. Mass ratio between canonical and Fe-corrected black hole mass versus redshift, colour-coded by accretion rate. The black solid lines show the mean mass ratio within the redshift range presented by the length of the line. The black error bars show the standard error of the mean mass ratio. The plot shows that the difference between the canonical and Fe-corrected mass increases as the redshift increases. The mean mass ratio in redshift bins $2 \leq z \leq 3$ and $z > 3$ differ at the $\sim 1.1\sigma$ level. On average, the high-z quasars ($z > 1$) have higher accretion rates.

SDSS spectra of the Shen et al. (2011) quasars with the log of the mass ratio ≥ 1, which appear as outliers in Fig. 7. Their spectra are consistent with the EV1 trend of strong relative strength of Fe II (see Appendix C).

Fig. 8 displays the mass ratio plotted against the Fe-corrected mass colour-coded by the Fe-corrected accretion rate. It shows the mean mass ratio in each mass bin for low- and high-z samples separately. The mean mass ratio and the standard error of the mean in each mass bin for the low-z sample are 0.71 ± 0.09 dex in $10^6 \leq M_{BH}(M_\odot) < 10^7$, 0.27 ± 0.01 dex in $10^7 \leq M_{BH}(M_\odot) < 10^8$, 0.125 ± 0.003 dex in $10^8 \leq M_{BH}(M_\odot) < 10^9$, 0.045 ± 0.004 dex in $10^9 \leq M_{BH}(M_\odot) < 10^{10}$, and -0.01 ± 0.01 dex in $M_{BH} \geq 10^{10} M_\odot$. The mean mass ratio and the standard error of mean in each mass bin for the high-z samples are 0.40 ± 0.03 dex in $10^8 \leq M_{BH}(M_\odot) < 10^9$, 0.27 ± 0.01 dex in $10^9 \leq M_{BH}(M_\odot) < 10^{10}$, and 0.26 ± 0.06 dex in $M_{BH} \geq 10^{11}(M_\odot)$. Fig. 8 demonstrates that the lower mass quasars ($M_{BH} < 10^8 M_\odot$) of the low-z Shen et al. (2011) sample have a higher accretion rate, hence, larger mass correction. For $M_{BH} \geq 10^8 M_\odot$, the mass correction is, on average, larger in the high-z samples compared to the low-z sample.

Plotting the change in black hole mass against redshift, colour-coded by accretion rate, Fig. 9 shows that, on average, the overestimation of mass increases as the redshift increases. The mean mass differences is 0.145 ± 0.003 dex for $z < 1$, 0.27 ± 0.01 dex for $1 < z < 2$, 0.30 ± 0.02 dex for $2 < z < 3$, and 0.37 ± 0.05 dex for $z > 3$. Fig. 9 also demonstrates that the high-z ($z > 1$) quasars on average have higher accretion rate black holes as compared to the low-z quasars, which include a large fraction of high-mass but low-accretion rate objects (also see mass vs accretion rate plot in the Section 5.1). It also shows that for $z > 1$, the fraction of high accretion rate quasars increases as redshift increases and their masses are overestimated by a factor of two to several using the canonical R–L relationship. Figs 8 and 9 show that the high-z quasars have larger masses and mass correction; they also have larger accretion rates on average (see Fig. 7) – the high-z quasars lack quasars with very weak Fe II that are present in large numbers in the low-redshift
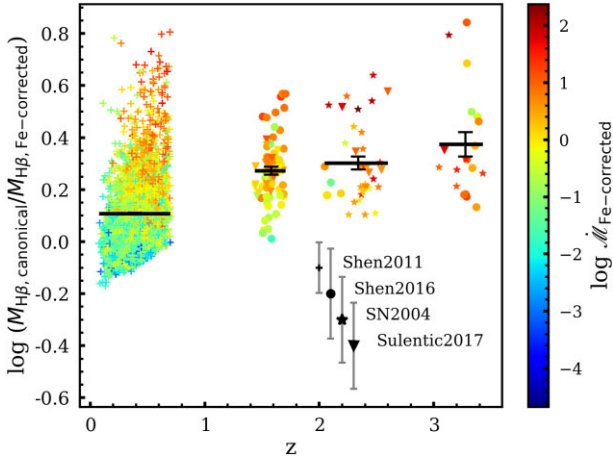
Figure 10. Same as Fig. 9 with only $M_{H\beta,\,\text{Fe-corrected}} > 10^8 M_\odot$ targets with $z < 0.7$.

Shen et al. (2011) sample (see the $\mathcal{R}_{\text{Fe}}$ distribution plot in the Section 5.1). This is likely a selection effect due to the difficulty of observing lower luminosity quasars at high z.

Fig. 10 is qualitatively the same as Fig. 9 but includes only $M_{\text{BH}} > 10^8 M_\odot$ quasars from the low-redshift Shen et al. (2011) sample. This eliminates 692 quasars with strong $\mathcal{R}_{\text{Fe}}$ and high accretion rate, giving a mean mass difference of 0.108 ± 0.003 dex for this low-z subsample. Fig. 10 demonstrates the stark difference the Fe-correction makes on the quasars with comparable black hole masses in the low- and high-redshift samples.

4.2 A stronger correlation between $\mathcal{R}_{\text{Fe}}$ and accretion rate parameters after using Fe-corrected mass

The dominant trend of decreasing EW[OIII] with the increasing $\mathcal{R}_{\text{Fe}}$ is known as EV1 (Boroson & Green 1992). It represents a correlation space in which many quasars properties correlate with the optical Fe II strength (Boroson & Green 1992; Boroson 2002). EV1 is primarily governed by the black hole accretion process parametrized by the Eddington ratio (Boroson & Green 1992; Marziani et al. 2001; Boroson 2002; Yuan & Wills 2003; Shen & Ho 2014; Sun & Shen 2015). The correlation between mass ratio and accretion rate parameters seen in Fig. 7 is largely due to this EV1 dependence.

Du et al. (2016, fig. 1) show the correlation between $\mathcal{R}_{\text{Fe}}$ and $L_{\text{Bol}}/L_{\text{Edd}}$ (also, $\dot{\mathcal{M}}$) for the SDSS DR5 sample of Hu et al. (2008) and RM AGNs. We plot versions of this correlation in Fig. 11 for our low- and high-z samples. The left-hand panel of Fig. 11 demonstrates that using an underestimated Eddington ratio based on the canonical black hole mass ($L_{\text{Bol}}/L_{\text{Edd}} \propto M_{\text{BH}}^{-1}$) gives a Pearson r correlation coefficient of only 0.31. The Fe-corrected black hole mass more accurately determines a higher Eddington ratio for the strong $\mathcal{R}_{\text{Fe}}$ emitters, improving the correlation to $r = 0.57$ (Fig. 11, middle panel). The right-hand panel of Fig. 11 shows the strongest correlation, $r = 0.61$, between $\mathcal{R}_{\text{Fe}}$ and Fe-corrected $\dot{\mathcal{M}}$. We recognize that the much larger correlation coefficient is in part an effect of self-correlation induced by the addition of $\mathcal{R}_{\text{Fe}}$ factor in the Du & Wang (2019) R-L relationship to estimate the Fe-corrected mass and consequently the Fe-corrected accretion rate parameters.

5 DISCUSSION

5.1 Selection biases and overall distribution of bright quasar properties

It is worth noting that the samples we use are not comprehensive and have selection effects. These samples, however, are likely representative of bright quasars at low and high redshifts and demonstrate the importance of the Fe-correction on the black hole mass estimates of highly accreting AGNs, especially at high redshift.

The luminosities and redshifts of the quasars we use depend on various selection effects, such as adopted S/N cuts and the wavelength of red-shifted H β and if it falls in a spectral window observable from the ground, as well as the properties of the quasar population itself. For instance, there are no extremely luminous quasars at low redshift, as only the lower mass objects are actively accreting, whereas at high redshift it is the most massive systems that are actively forming, a phenomenon known as 'downsizing' (Heckman et al. 2004; Hasinger, Miyaji & Schmidt 2005). To show these and other effects, we plot the mass–luminosity plane for all our samples in Fig. 12. We see that there are quasars accreting at or slightly above the Eddington luminosity in both the low- and high-redshift samples, but they are of intrinsically different masses and luminosity. Furthermore, it is only a small fraction of the low-redshift quasars that show such high accretion rates, as compared to the high-redshift samples. There are de facto luminosity cuts for the lowest mass black holes ($<10^8 M_\odot$),
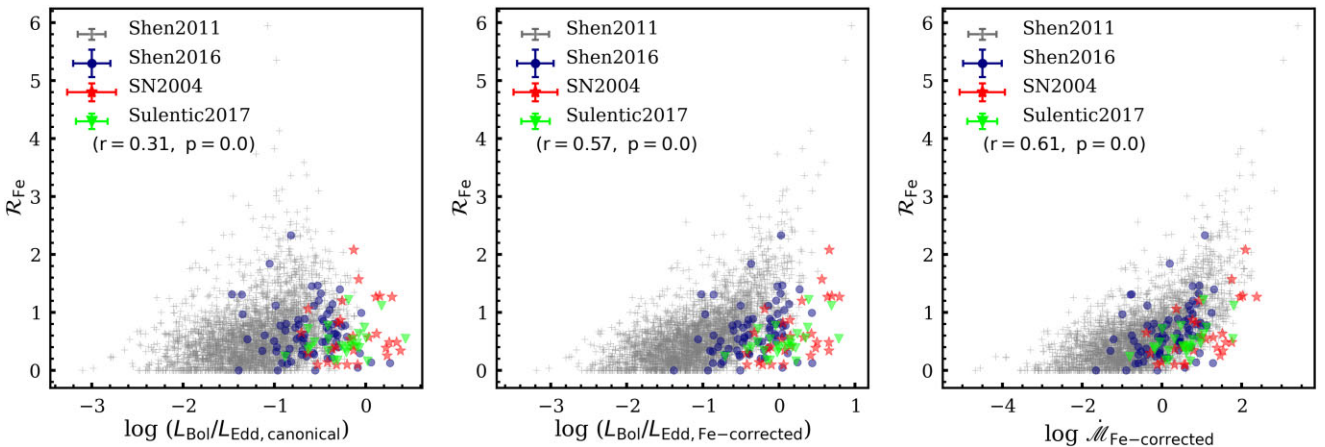

Figure 11. $\mathcal{R}_{\text{Fe}}$ versus canonical Eddington ratio (left), Fe-corrected Eddington ratio (middle), and Fe-corrected $\dot{\mathcal{M}}$ (right). The Pearson correlation coefficients r and p are given in parentheses.

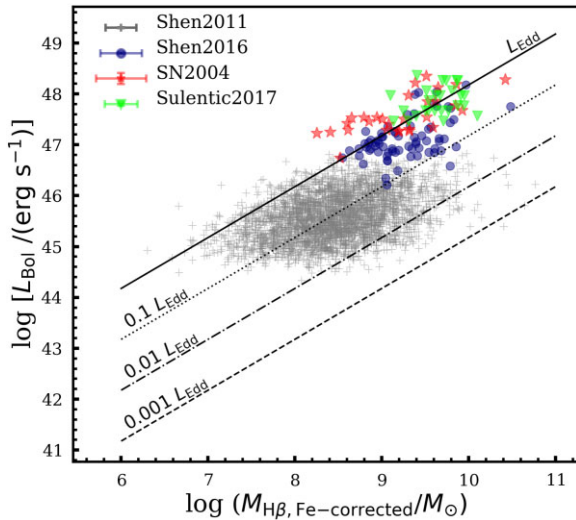**Figure 12.** Bolometric luminosity versus Fe-corrected black hole mass for all samples. The black solid line represents the $L_{Bol} = L_{Edd}$, the dotted line represents $L_{Bol} = 0.1L_{Edd}$, the dot–dashed line represents $L_{Bol} = 0.01L_{Edd}$, and the dashed line represents $L_{Bol} = 0.001L_{Edd}$.

which must be accreting at Eddington ratios greater than ∼0.1 to be luminous enough to be included in the sample. The near-IR spectral surveys naturally chose the brightest objects known at high redshift, which correspond to the most luminous and highest accretion rate quasars with the largest black hole masses. There is also a de facto accretion rate limit below ∼0.01 of the Eddington ratio, where active galaxies stop displaying broad emission lines (e.g. Guolo et al. 2021, and references within).

Fig. 13 plots our Fe-corrected black hole masses against our accretion rate indicators, and features a colour scheme to identify the values of $\mathcal{R}_{Fe}$ across the plane. The super-Eddington accreting quasars in both low- and high-redshift samples in general display the largest $\mathcal{R}_{Fe}$ measurements. The quasars with large black hole masses and the lowest accretion rates in general display the smallest $\mathcal{R}_{Fe}$ measurements. We show the distribution of $\mathcal{R}_{Fe}$ in the low-z and the combined high-z samples in Fig. 14. To illustrate the diversity in accretion rates of low-z quasars, we further divided the low-z sample into low and high mass. There are 692 out of 3309 quasars in the low-z sample with a mass less than $10^8 M_\odot$, while the remaining 79 per cent have a mass $\geq 10^8 M_\odot$. We excluded 11 quasars in the low-mass low-z sample (spectra shown in Appendix B) that have $\mathcal{R}_{Fe} > 3$. Fig. 14 demonstrates that low-mass, low-z quasars have higher accretion rates (Fig. 13) and stronger $\mathcal{R}_{Fe}$ (Fig. 14). They are the low-mass analogues of massive highly accreting quasars at high z, albeit less massive and less luminous. On the other hand, the high-mass quasars in the low-z sample have lower accretion rates and smaller $\mathcal{R}_{Fe}$ measurements. The distribution of $\mathcal{R}_{Fe}$ in the high-z quasars shows that they consist of strong Fe II emitters and generally lack quasars with very small or zero $\mathcal{R}_{Fe}$.

5.2 Importance of the $\mathcal{R}_{Fe}$ correction

Two dimensionless quantities commonly used to parametrize the black hole's accretion rate are Eddington ratio (L_{Bol}/L_{Edd}) and $\dot{\mathcal{M}}$. With the increasing number of RM measurements, many studies use these quantities to correct the R-L relationship for accretion-rate dependence. Fonseca Alvarez et al. (2020) point out that correlations between an R_{BLR} offset, i.e. the difference between R_{BLR} from

RM measurement and one estimated from R-L relationship, and accretion rate estimators suffer from self-correlation. The R_{BLR} offset is proportional to the ratio of $R/L^{0.5}$, $L_{Bol}/L_{Edd} \propto L_{5100\text{Å}}/R$, and $\dot{\mathcal{M}} \propto L_{5100\text{Å}}^{1.5}/R^2$. Therefore, using an independent estimate of accretion rate like $\mathcal{R}_{Fe}$ is better. A strong anticorrelation is seen between the BLR size offset and $\mathcal{R}_{Fe}$ for RM AGNs in the SEAMBH sample (Du et al. 2018; Du & Wang 2019). Grier et al. (2017), however, studied their H β SDSS-RM sample and did not find this anticorrelation (Fonseca Alvarez et al. 2020). The H β SDSS-RM sample has a median $L_{Bol}/L_{Edd} \sim 0.1$ (Shen et al. 2019) and lacks extremely high accretors. For low-accreting AGNs, both accretion rate and, perhaps, black hole spin govern the BLR size (Wang et al. 2014a; Du et al. 2018). After dividing the SDSS-RM sample into high and low accretion rate, Du et al. (2018) show that the high accretion rate subsample follows the expected anticorrelation between the BLR size offset and $\mathcal{R}_{Fe}$ (see fig. 5 of Du et al. 2018).

Our results demonstrate the significant impact of including $\mathcal{R}_{Fe}$ in the R-L relationship on the determination of black hole mass and accretion rate parameters. Such accretion-rate-based correction is crucial for luminous broad-absorption line (BAL) quasars that are known to have strong Fe II (Turnshek et al. 1997; Boroson 2002; Yuan & Wills 2003; Runnoe et al. 2013a, and references therein). We found that the strongest Fe-emitters in general have higher accretion rate, and consequently overestimated black hole mass. Quasars with $L_{Bol}/L_{Edd} \geq 1$ can have black hole mass overestimated by up to an order of magnitude (as shown in Fig. 7).

5.3 Some caveats for black hole mass estimation

We made some choices, depending on the availability of data, that impacted our results. Past studies interchangeably used flux ratio and EW ratio to define $\mathcal{R}_{Fe}$. To check how much this impacts estimates of black hole mass, we evaluated the change in $\mathcal{R}_{Fe}$ using each of these two quantities, in turn, to estimate black hole masses for the Shen et al. (2011) sample. They tabulate EWs of H β and Fe II. We used the given EW and line luminosity for H β to compute the continuum luminosity at 4861Å. We scaled the continuum luminosity to the mean wavelength of Fe II i.e. 4560Å using the slope for the H β region and calculated the line luminosity for Fe II. The mean percentage difference between $\mathcal{R}_{Fe}$ measured from line luminosity ratios and EW ratios is 3.2 ± 0.1 per cent and the standard deviation is ∼4 per cent.

The FWHM and line dispersion, σ_{line}, both used as a proxy for velocity width in the virial mass formula, have their pros and cons. All the samples we used have available FWHM measurements of the H β line as its measurement has been more common than σ_{line} in catalogues. FWHM is also less sensitive to line wings and blending with narrow lines (Peterson et al. 2004). But, for at least the radio-loud subclass, FWHM is known to correlate with quasar orientation (Wills & Browne 1986). Dalla Bontà et al. (2020) show that for H β both FWHM and σ_{line} provide reasonable proxies, with σ_{line} being slightly better. Some other investigations indicate that σ_{line} gives better virial mass estimates; for example, Peterson et al. (2004) find a tighter virial correlation when using σ_{line}, and Denney et al. (2013) find that H β- and C IV-based mass agree better when using σ_{line}. Collin et al. (2006) compare virial black hole mass based on different line-width measurements with black hole mass from the stellar velocity dispersion of RM AGNs. They find that the σ_{line}-based mass is better, albeit at low statistical significance. Recently, Wang et al. (2019) presented a similar study using the SDSS-RM quasars and reported that although FWHM suffers from orientation effects more than σ_{line}, the use of σ_{line} does not guarantee a better
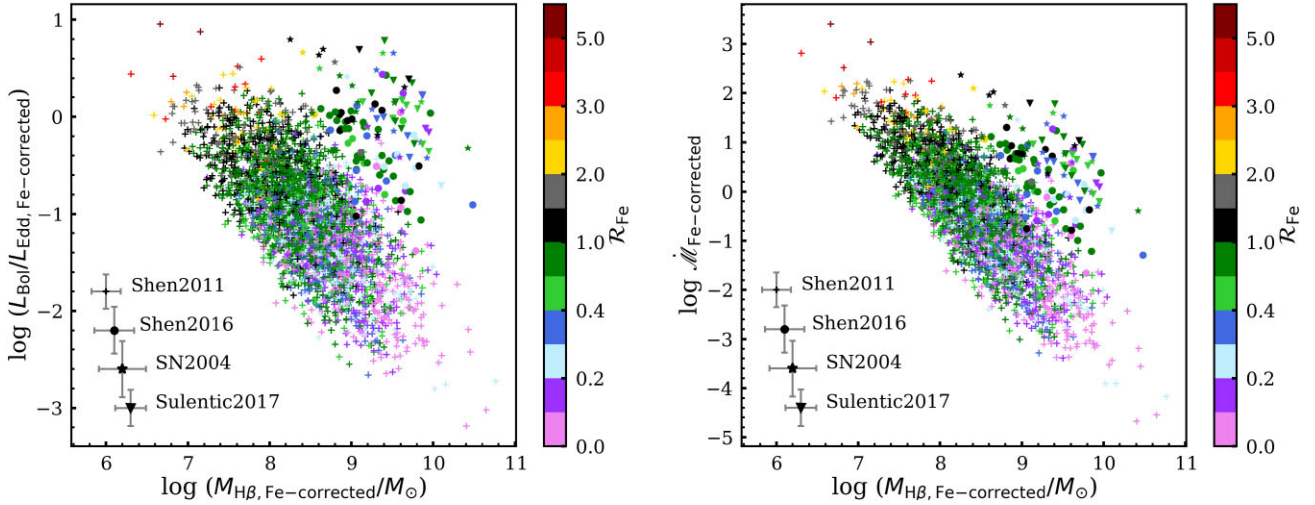
Figure 13. Fe-corrected mass versus accretion rate parameter colour-coded by $\mathcal{R}_{Fe}$.
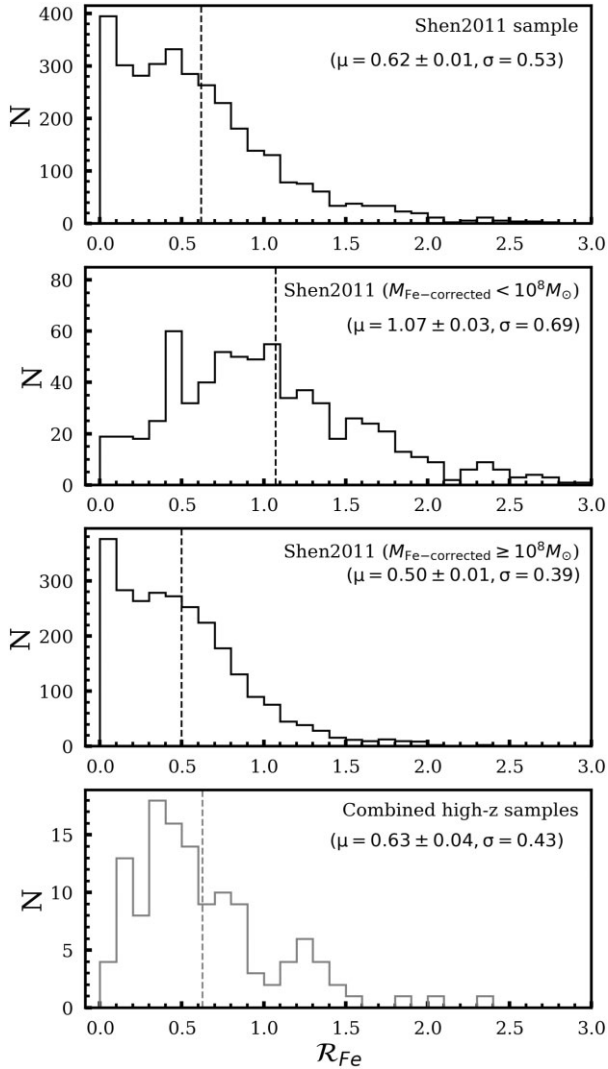

Figure 14. Distribution of $\mathcal{R}_{Fe}$ in low-redshift subsamples of Shen et al. 2011 (top three panels) and all the high-redshift samples combined together (bottom panel). The plot excludes targets with $\mathcal{R}_{Fe} > 3$.

virial mass estimate. An anticorrelation between FWHM and the virial coefficient is known, and using a constant value for f introduces additional uncertainty to the mass estimates (Mejía-Restrepo et al. 2018).

If the average viewing angle in the low-z RM sample differs from that in luminous bright high-z quasars, this could introduce an additional bias in the black hole mass estimates. The virial coefficient f very likely correlates with inclination angle (Collin et al. 2006; Pancoast et al. 2014).

A couple of possible competing orientation effects can introduce systematic biases that we may investigate in the future. For example, there is an observational bias due to the anisotropic nature of an accretion disc. The continuum emission varies with orientation (e.g. Runnoe, Shang & Brotherton 2013c): a face-on disc is brighter than a relatively edge-on disc leading to a selection bias towards more face-on sources in luminous high-z samples (DiPompeo et al. 2014). Although, if the selection is entirely random, we should observe more relatively edge-on sources because of the higher probability of line of sight being edge-on than face-on. These factors must be considered along with the likelihood that AGN opening angles increase with increasing luminosity (e.g. Lawrence 1991; Ma & Wang 2013).

It is worth noting that the RM mass has an inherent uncertainty of 0.3–0.5 dex due to its calibration against the M–$\sigma_\star$ relation (Peterson 2010; Vestergaard et al. 2011; Shen 2013; Ho & Kim 2014). The SE mass estimates have a 0.5–0.6 dex relative uncertainty and 0.7 dex absolute uncertainty (e.g. table 5, Vestergaard & Peterson 2006).

Our updated SE mass prescription using the $\mathcal{R}_{Fe}$-based correction will not improve the precision of the estimate in individual objects, but will improve the accuracy, particularly for those with high accretion rates, which otherwise would be systematically overestimated. While the correction will generally be smaller than the overall absolute uncertainty, correcting for systematic effects is important.

6 CONCLUSIONS AND FUTURE OUTLOOK

The recently established R-L relation by Du & Wang (2019) takes into account the bias due to the accretion rate using $\mathcal{R}_{Fe}$. We use quasar samples across a wide range of redshifts from Shemmer et al. (2004, 2010), Netzer et al. (2004), Shen et al. (2011), Shen (2016), and Sulentic et al. (2017) to characterize the bias in black hole mass and accretion rate when using the canonical and

Du & Wang (2019) R-L relationships. The single-epoch black hole mass estimates using the canonical R-L relationship systematically overestimate the mass of the black hole and underestimate the accretion rate. At high redshift, the black hole mass has likely been overestimated by a factor of two on average when using the canonical R-L relationship. The overestimation could be up to an order of magnitude for the most highly accreting quasars, likely the most luminous such objects in the early Universe. Our results also indicate that the high-redshift luminous quasars have highly accreting black holes whose optical spectra have characteristically strong $\mathcal{R}_{Fe}$. The low-redshift analogues of these highly accreting quasars are less massive but also exhibit strong $\mathcal{R}_{Fe}$. The use of the canonical R-L relationship results in an overestimation of black hole mass by a factor of two, on average, for both these highly accreting quasar populations.

The largest galaxy interactions/growth and star formation rates occur at cosmic noon, along with the most luminous quasars that will preferentially have very high accretion rates. Kelly & Shen (2013) show that the fraction of highly accreting AGNs increases with increasing redshift. The gas fraction in AGN host galaxies increases with redshift, likely contributing to the higher accretion rates (Shirakata et al. 2019). Hence, the mass and accretion rate corrections are relatively common among the most luminous quasars at cosmic noon, and likely the case at even higher redshifts. Low-accretion rate AGNs likely exist at these redshifts but are more commonly below the the flux limits of surveys like SDSS, or only have low S/N spectra currently available (e.g. Kelly & Shen 2013).

In the absence of rest-frame optical spectra for high-redshift objects, Mg II and C IV provide an alternative for black hole mass estimation. Such mass estimates assume that the emission line follows normal 'breathing', i.e. as continuum luminosity increases, the time lag between continuum and emission-line variation increases, and the emission-line width decreases. Only the Hβ line truly follows this; Mg II shows no breathing, whereas C IV shows antibreathing (Wang et al. 2020). To correctly determine the black hole mass and accretion rate for high-redshift quasars, we need more near-IR spectroscopic surveys to facilitate direct checks using the Hβ line. In the future, the Gemini Near-Infrared Spectrograph-Distant Quasar Survey (Matthews et al. 2021) will provide a large, uniformly distributed sample of quasars at high redshift. It will provide measurements of Hβ, Fe II, [O III], and other UV lines that fall in the near-IR regions. The final data set will have a high signal-to-noise ratio (S/N $\sim$ 35) in the observed-frame $\sim$ 0.8–2.5 μm band for a few hundred SDSS quasars at $1.5 \leq z \leq 3.5$. The wavelength coverage of the survey may enable the use of the C IV line and other UV features to determine an $\mathcal{R}_{Fe}$ equivalent in the near-IR.

The presence of a billion solar mass quasar at $z > 6$ is a problem because it is challenging to create and provide constant feeding of the black hole when the Universe was less than a billion years old (Turner 1991; Haiman & Loeb 2001; Shen 2013; Inayoshi, Visbal & Haiman 2020). Our results indicate that the black hole masses of high-redshift quasars are typically overestimated, especially for the most highly accreting black holes. Understanding the formation and evolution of massive black holes in the early Universe necessitates taking into consideration $\mathcal{R}_{Fe}$-based accretion rate bias in their black hole mass estimates.

ACKNOWLEDGEMENTS

DATA AVAILABILITY

The data underlying this article are available in Shen et al. (2011) (DOI: 10.1088/0067-0049/194/2/45), Shen (2016) (DOI: 10.3847/0004-637X/817/1/55), Shemmer et al. (2004) (DOI: 10.1086/423607), Netzer et al. (2004) (DOI: 10.1086/423608), Sulentic et al. (2017) (10.1051/0004-6361/201630309), and Shemmer et al. (2010) (DOI: 10.1088/2041-8205/722/2/L152). See Section 3 for the sample selection criteria applied.

REFERENCES

Abazajian K. N. et al., 2009, ApJS, 182, 543
Bentz M. C., Katz S., 2015, PASP, 127, 67
Bentz M. C., Peterson B. M., Pogge R. W., Vestergaard M., Onken C. A., 2006, ApJ, 644, 133
Bentz M. C., Peterson B. M., Netzer H., Pogge R. W., Vestergaard M., 2009, ApJ, 697, 160
Bentz M. C. et al., 2013, ApJ, 767, 149
Blandford R. D., McKee C. F., 1982, ApJ, 255, 419
Boroson T. A., 2002, ApJ, 565, 78
Boroson T. A., Green R. F., 1992, ApJS, 80, 109
Brotherton M. S., Runnoe J. C., Shang Z., DiPompeo M. A., 2015, MNRAS, 451, 1290
Collin S., Kawaguchi T., Peterson B. M., Vestergaard M., 2006, A&A, 456, 75
Collinge M. J. et al., 2005, AJ, 129, 2542
Dalla Bontà E. et al., 2020, ApJ, 903, 112
Davies F. B., Hennawi J. F., Eilers A.-C., 2019, ApJ, 884, L19
Denney K. D., Peterson B. M., Dietrich M., Vestergaard M., Bentz M. C., 2009, ApJ, 692, 246
Denney K. D., Pogge R. W., Assef R. J., Kochanek C. S., Peterson B. M., Vestergaard M., 2013, ApJ, 775, 60
DiPompeo M. A., Myers A. D., Brotherton M. S., Runnoe J. C., Green R. F., 2014, ApJ, 787, 73
Du P., Wang J.-M., 2019, ApJ, 886, 42
Du P. et al., 2014, ApJ, 782, 45
Du P. et al., 2015, ApJ, 806, 22
Du P., Wang J.-M., Hu C., Ho L. C., Li Y.-R., Bai J.-M., 2016, ApJ, 818, L14
Du P. et al., 2018, ApJ, 856, 6
Fonseca Alvarez G. et al., 2020, ApJ, 899, 73
Grier C. J. et al., 2017, ApJ, 851, 21
Guolo M., Ruschel-Dutra D., Grupe D., Peterson B. M., Storchi-Bergmann T., Schimoia J., Nemmen R., Robinson A., 2021, MNRAS, 508, 144
Haiman Z., Loeb A., 2001, ApJ, 552, 459
Hasinger G., Miyaji T., Schmidt M., 2005, A&A, 441, 417
Heckman T. M., Kauffmann G., Brinchmann J., Charlot S., Tremonti C., White S. D. M., 2004, ApJ, 613, 109
Ho L. C., Kim M., 2014, ApJ, 789, 17
Hogg D. W., Baldry I. K., Blanton M. R., Eisenstein D. J., 2002, preprint (arXiv:astro–ph/0210394)
Hu C., Wang J.-M., Ho L. C., Chen Y.-M., Zhang H.-T., Bian W.-H., Xue S.-J., 2008, ApJ, 687, 78
Inayoshi K., Visbal E., Haiman Z., 2020, ARA&A, 58, 27
Johnson J. L., Whalen D. J., Fryer C. L., Li H., 2012, ApJ, 750, 66
Kaspi S., Smith P. S., Netzer H., Maoz D., Jannuzi B. T., Giveon U., 2000, ApJ, 533, 631

Kaspi S., Maoz D., Netzer H., Peterson B. M., Vestergaard M., Jannuzi B. T., 2005, ApJ, 629, 61

Kaspi S., Brandt W. N., Maoz D., Netzer H., Schneider D. P., Shemmer O., 2007, ApJ, 659, 997

Kaspi S., Brandt W. N., Maoz D., Netzer H., Schneider D. P., Shemmer O., Grier C. J., 2021, ApJ, 915, 129

Kelly B. C., Shen Y., 2013, ApJ, 764, 45

Kormendy J., Ho L. C., 2013, ARA&A, 51, 511

Laor A., 1998, ApJ, 505, L83

Lawrence A., 1991, MNRAS, 252, 586

Lodato G., Natarajan P., 2006, MNRAS, 371, 1813

Ma X.-C., Wang T.-G., 2013, MNRAS, 430, 3445

Martínez-Aldama M. L., Zajaček M., Czerny B., Panda S., 2020, ApJ, 903, 86

Marziani P., Sulentic J. W., Zwitter T., Dultzin-Hacyan D., Calvani M., 2001, ApJ, 558, 553

Marziani P., Sulentic J. W., Stirpe G. M., Zamfir S., Calvani M., 2009, A&A, 495, 83

Matthews B. M. et al., 2021, ApJS, 252, 15

McIntosh D. H., Rieke M. J., Rix H. W., Foltz C. B., Weymann R. J., 1999, ApJ, 514, 40

Mejía-Restrepo J. E., Lira P., Netzer H., Trakhtenbrot B., Capellupo D. M., 2018, Nat. Astron., 2, 63

Mineshige S., Kawaguchi T., Takeuchi M., Hayashida K., 2000, PASJ, 52, 499

Mortlock D. J. et al., 2011, Nature, 474, 616

Netzer H., Peterson B. M., 1997, in Maoz D., Sternberg A., Leibowitz E. M., eds, Astronomical Time Series. Kluwer, Dordrecht, p. 85

Netzer H., Shemmer O., Maiolino R., Oliva E., Croom S., Corbett E., di Fabrizio L., 2004, ApJ, 614, 558

Onken C. A., Ferrarese L., Merritt D., Peterson B. M., Pogge R. W., Vestergaard M., Wandel A., 2004, ApJ, 615, 645

Pancoast A., Brewer B. J., Treu T., Park D., Barth A. J., Bentz M. C., Woo J.-H., 2014, MNRAS, 445, 3073

Peterson B. M., 1993, PASP, 105, 247

Peterson B. M., 2010, in Peterson B. M., Somerville R. S., Storchi-Bergmann T., eds, Proc. IAU Symp. 267, Co-Evolution of Central Black Holes and Galaxies. Kluwer, Dordrecht, p. 151

Peterson B. M., 2014, Space Sci. Rev., 183, 253

Peterson B. M. et al., 2004, ApJ, 613, 682

Richards G. T. et al., 2006, ApJS, 166, 470

Runnoe J. C., Ganguly R., Brotherton M. S., DiPompeo M. A., 2013a, MNRAS, 433, 1778

Runnoe J. C., Brotherton M. S., Shang Z., DiPompeo M. A., 2013b, MNRAS, 434, 848

Runnoe J. C., Shang Z., Brotherton M. S., 2013c, MNRAS, 435, 3251

Shakura N. I., Sunyaev R. A., 1973, A&A, 500, 33

Shemmer O., Netzer H., Maiolino R., Oliva E., Croom S., Corbett E., di Fabrizio L., 2004, ApJ, 614, 547

Shemmer O. et al., 2010, ApJ, 722, L152

Shen Y., 2013, Bull. Astron. Soc. India, 41, 61

Shen Y., 2016, ApJ, 817, 55

Shen Y., Ho L. C., 2014, Nature, 513, 210

Shen Y., Liu X., 2012, ApJ, 753, 125

Shen Y., Greene J. E., Strauss M. A., Richards G. T., Schneider D. P., 2008, ApJ, 680, 169

Shen Y. et al., 2011, ApJS, 194, 45

Shen Y. et al., 2015, ApJS, 216, 4

Shen Y. et al., 2019, ApJS, 241, 34

Shirakata H., Kawaguchi T., Oogi T., Okamoto T., Nagashima M., 2019, MNRAS, 487, 409

Sulentic J. W., Stirpe G. M., Marziani P., Zamanov R., Calvani M., Braito V., 2004, A&A, 423, 121

Sulentic J. W., Repetto P., Stirpe G. M., Marziani P., Dultzin-Hacyan D., Calvani M., 2006, A&A, 456, 929

Sulentic J. W. et al., 2017, A&A, 608, A122

Sun J., Shen Y., 2015, ApJ, 804, L15

Trakhtenbrot B., Volonteri M., Natarajan P., 2017, ApJ, 836, L1

Turner E. L., 1991, AJ, 101, 5

Turnshek D. A., Monier E. M., Sirola C. J., Espey B. R., 1997, ApJ, 476, 40

van Groningen E., Wanders I., 1992, PASP, 104, 700

Vestergaard M., Peterson B. M., 2006, ApJ, 641, 689

Vestergaard M., Denney K., Fan X., Jensen J. J., Kelly B. C., Osmer P. S., Peterson B., Tremonti C. A., 2011, PoS, NLS1, 038

Volonteri M., Silk J., Dubus G., 2015, ApJ, 804, 148

Wandel A., Peterson B. M., Malkan M. A., 1999, ApJ, 526, 579

Wang J.-M., Szuszkiewicz E., Lu F.-J., Zhou Y.-Y., 1999, ApJ, 522, 839

Wang J.-M., Du P., Li Y.-R., Ho L. C., Hu C., Bai J.-M., 2014a, ApJ, 792, L13

Wang J.-M. et al., 2014b, ApJ, 793, 108

Wang S. et al., 2019, ApJ, 882, 4

Wang S. et al., 2020, ApJ, 903, 51

Wang F. et al., 2021, ApJ, 907, L1

Wills B. J., Browne I. W. A., 1986, ApJ, 302, 56

Wisotzki L., Christlieb N., Bade N., Beckmann V., Köhler T., Vanelle C., Reimers D., 2000, A&A, 358, 77

Yu L.-M., Bian W.-H., Wang C., Zhao B.-X., Ge X., 2019, MNRAS, 488, 1519

Yu L.-M., Zhao B.-X., Bian W.-H., Wang C., Ge X., 2020a, MNRAS, 491, 5881

Yu L.-M., Bian W.-H., Zhang X.-G., Zhao B.-X., Wang C., Ge X., Zhu B.-Q., Chen Y.-Q., 2020b, ApJ, 901, 133

Yuan M. J., Wills B. J., 2003, ApJ, 593, L11

APPENDIX A: SELECTION CRITERIA PRODUCING THE HIGH-Z SUBSAMPLES

(i) Shen (2016) catalogued the properties of 74 quasars in the redshift range $1.5 \leq z \leq 3.5$. 60/74 targets are from Shen & Liu (2012) in the redshift range 1.5 to 2.2, and 14 new quasars at $z \sim 3.3$ were added by Shen (2016). All targets were selected from the SDSS DR7 quasar catalogue to have an S/N >10 in the C IV through the Mg II spectral regions. They excluded targets with broad absorption features or unusual continuum shapes. Such selection criteria at high redshift result in a sample of very luminous quasars, yet they demonstrate similar diversity in spectral features as seen in low-z quasars (Shen & Liu 2012; Shen 2016). Fig. 3 of Shen (2016) presents the median spectrum of these 74 quasars. The median spectrum shows broader H β and Hα lines characteristic of massive black holes as compared to the low-z quasars. These quasars span nearly the entire range of $\mathcal{R}_{\mathrm{Fe}}$, and follow the EV1 trends seen in the low-z quasars (Shen 2016, figs 7 and 8).

(ii) The SN2004 sample includes 29 quasars in the redshift range $2 \leq z \leq 3.5$. They selected luminous quasars ($L \geq 10^{46}\,\mathrm{erg\ s^{-1}}$) with H magnitudes ≤ 17 allowing them to obtain high S/N IR spectra. These quasars had archival UV spectra including the N V and C IV emission lines without severe absorption. Their selection criteria also required the H β line to be unaffected by atmospheric absorption in the IR bands. Shemmer et al. (2004) show the spectrum of these quasars in their figs 1, 2, and 3. These high-z quasars also follow the EV1 trend; in fact, they occupy the same region on the $\mathcal{R}_{\mathrm{Fe}}$ versus $L_{\mathrm{Bol}}/L_{\mathrm{Edd}}$ plot as the narrow-line Seyfert 1 galaxies from Boroson & Green (1992) (Netzer et al. 2004, Fig. 8).

(iii) Sulentic et al. (2017) selected 28 quasars from the magnitude-limited ($m_{\mathrm{B}} \approx 17.5$) Hamburg ESO survey (Wisotzki et al. 2000) with $z > 1.4$ to allow observation of the C IV spectral region. They are high-luminosity ($\log L_{5100\text{Å}} > 46\ \mathrm{erg\ s^{-1}}$) quasars with the H β region properties reported by Sulentic et al. (2004, 2006) and Marziani et al. (2009). Two quasars in Sulentic et al. (2017) are known to be gravitationally lensed, another is a mini-broad absorption line quasar, and two are weak-line quasars (WLQs).

APPENDIX B: WEAK-LINE QUASARS

With the assumption that virial mass method holds true for WLQs, we show the effect of the Fe-correction on the determination of their black hole mass. Our analysis includes four WLQs, two from Sulentic et al. (2017) and two from Shemmer et al. (2010).

We discussed the sample selection criterion of Sulentic et al. (2017) in Appendix A; their WLQs have redshifts 1.52 and 1.58. WLQs in the Shemmer et al. (2010) sample are at a redshift of 3.49 and 3.55 and were selected from Collinge et al. (2005) for near-IR spectroscopy as their H β regions fall in the middle of the *K* band. These latter WLQs show weaker H β lines (Shemmer et al. 2010, fig. 2) in comparison to high-*z* quasars with similar luminosities, but have reliable measurements of the parameters used for black hole mass estimates (Shemmer et al. 2010). Shemmer et al. (2010) suggest the weakness of low- and high-ionization emission lines is due to a gas deficiency in the BLR indicated by a low BLR covering factor rather than an effect of extreme accretion rate. The H β lines in WLQs from Sulentic et al. (2017) are of normal strength.

After utilizing the Du & Wang (2019) R-L relationship, Fig. B1 (left) shows that the two WLQs from Shemmer et al. (2010) sample have extreme accretion rates, and their mass overestimated by a factor of ~14. The two WLQs from Sulentic et al. (2017) show a mass overestimation of a factor of ~2.5. Although Fe-correction is crucial for all four WLQs as they have strong Fe II, the effect of Fe-correction is most extreme in the WLQs with weaker H β lines ($\mathcal{R}_{Fe} \propto 1$/EW H$\beta$) from Shemmer et al. (2010) in comparison to the WLQs from Sulentic et al. (2017). However, WLQs with weak H β lines in Shemmer et al. (2010) have larger measurement uncertainties associated with their FWHM and EW of H β measurements and hence larger measurement errors in masses. The mass ratio versus redshift plot (Fig. B1 right) does not have a significant change in mean mass ratio in the redshift bin by the inclusion of just two WLQs. The mean mass differences are 0.14 ± 0.00 dex for $z < 1$, 0.28 ± 0.01 dex for $1 < z < 2$, 0.30 ± 0.02 dex for $2 < z < 3$, and 0.45 ± 0.07 dex for $z > 3$.

APPENDIX C: SDSS SPECTRA OF HIGHLY ACCRETING QUASARS IN SHEN ET AL. (2011)

Table C1 lists the name, EW of H β, EW of Fe II, $\mathcal{R}_{Fe}$, and log of mass ratio i.e. $\log(M_{H\beta,\,canonical}/M_{H\beta,\,Fe\text{-corrected}})$ of Shen et al. (2011) quasars that appear as outliers (log of mass ratio >1) in Figs 7, 8, and 9. Fig. C1 shows the SDSS spectra of these quasars arranged in descending order of mass ratio. SDSS J152350.42+391405.2 shows broad absorption line features.
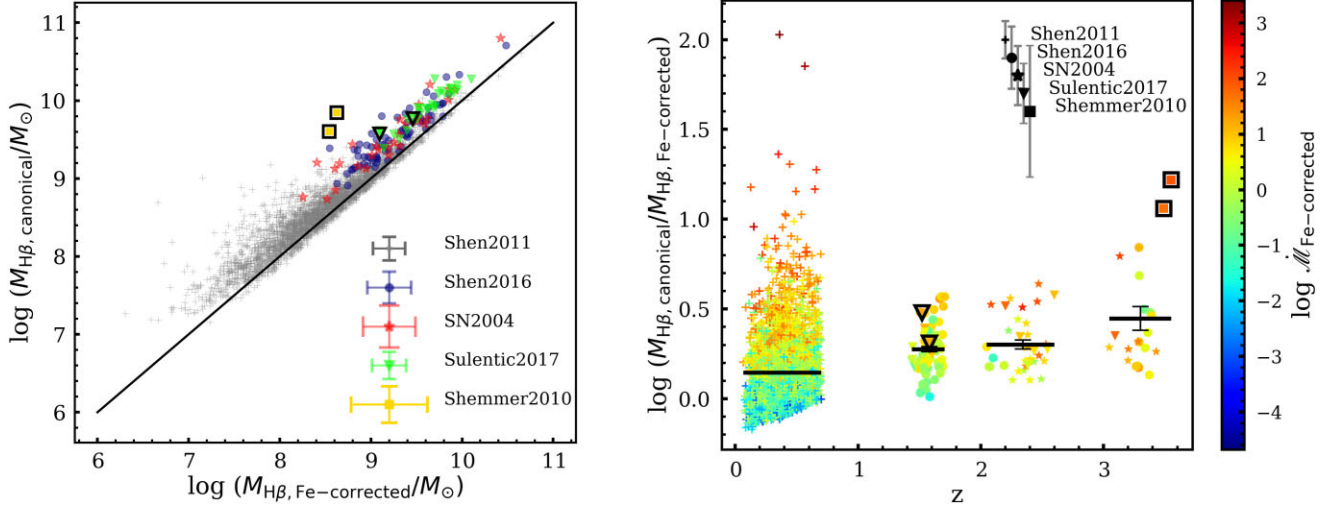

Figure B1. Left-hand panel: Black hole mass calculated using the canonical (*y*-axis) and Fe-corrected (*x*-axis) R-L relations. Right-hand panel: Mass ratio between canonical and Fe-corrected black hole mass versus redshift colour-coded by accretion rate. In both plots, WLQs are outlined in black.

Table C1. Outliers in Shen et al. (2011) sample.

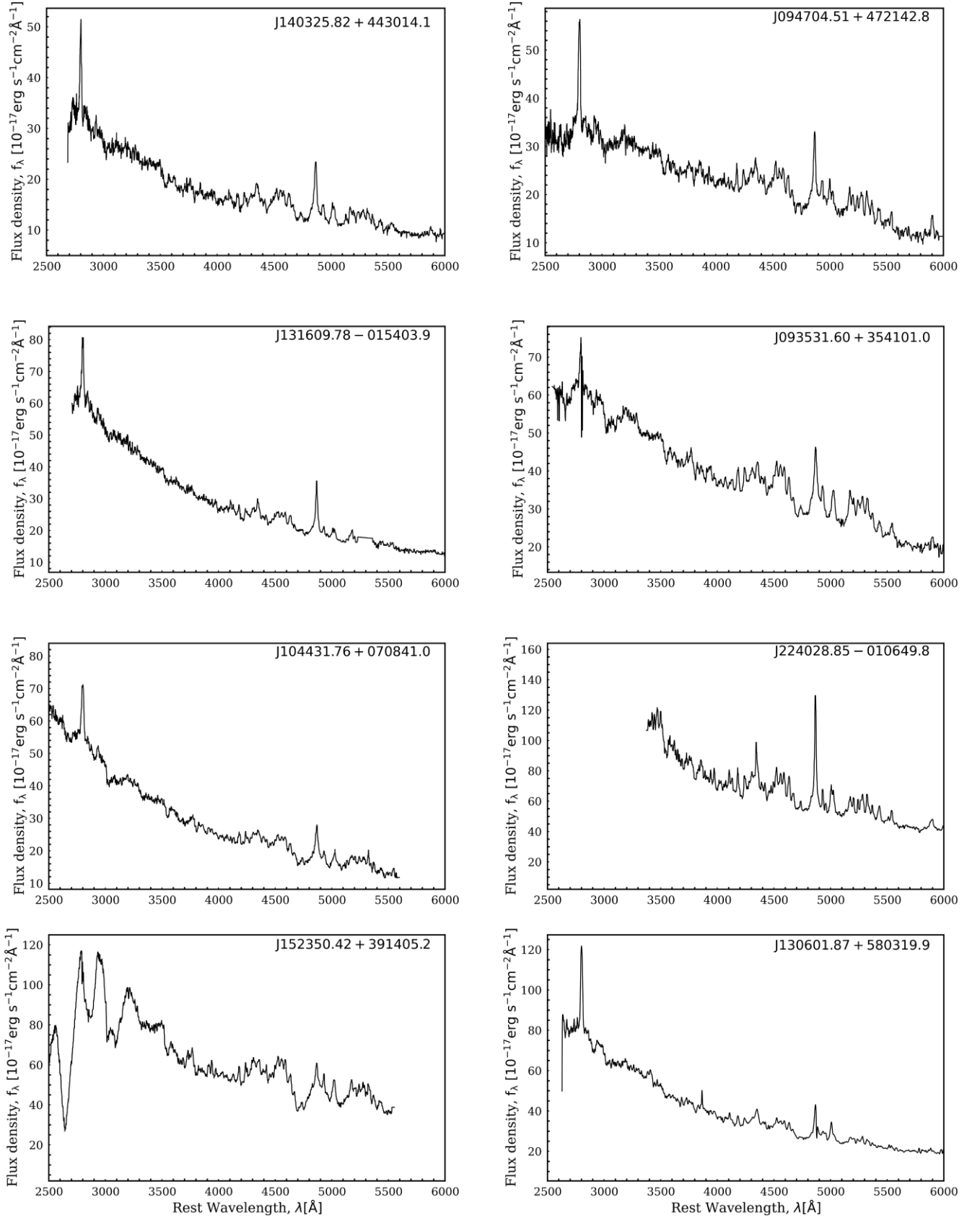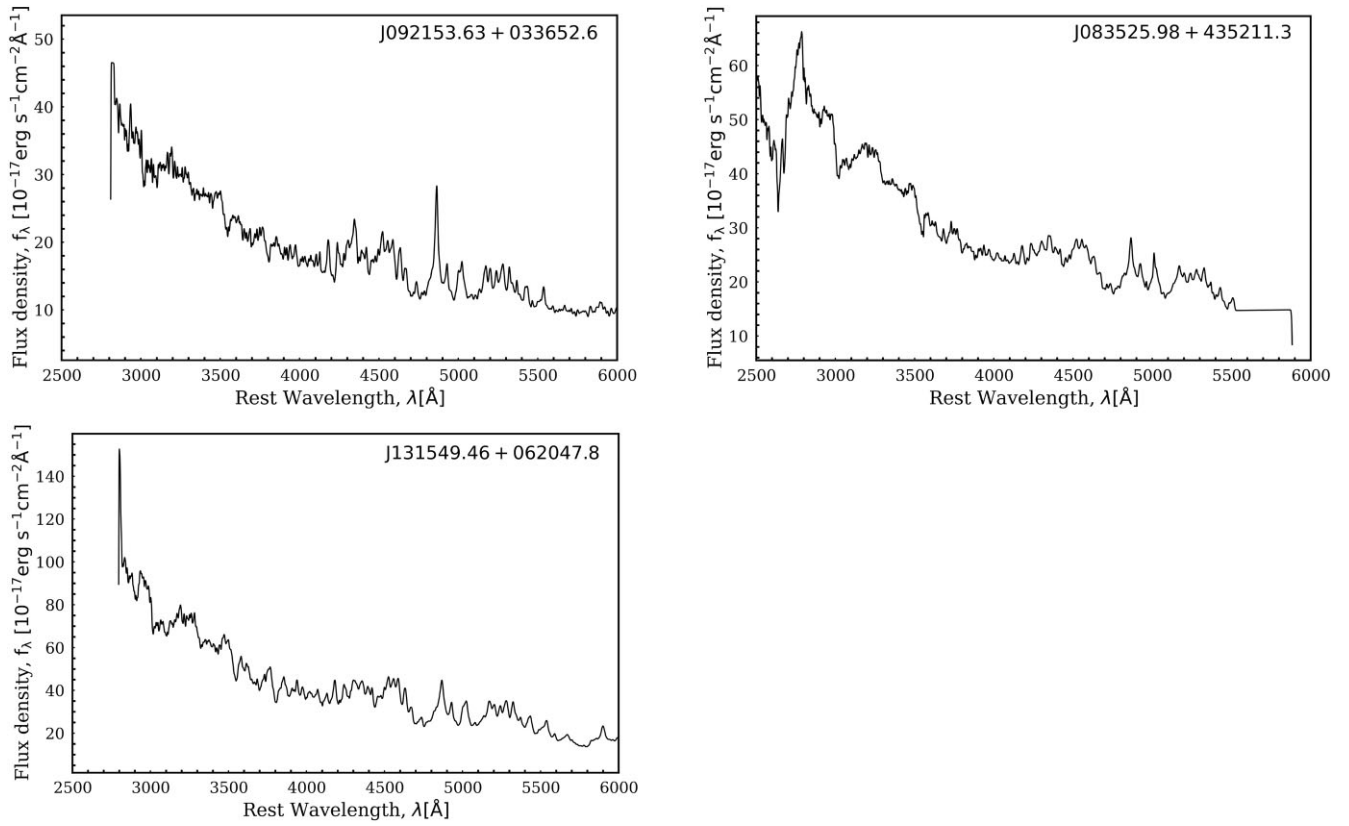| SDSSJ	z	EW(Hβ) (Å)	EW(FeII) (Å)	$\mathcal{R}_{Fe}$	log(Mass ratio) (dex)
J140325.82+443014.1	0.4122	28.6	89.3	3.12	1.02
J094704.51+472142.8	0.5392	26.9	81.1	3.01	1.03
J131609.78−015403.9	0.4057	14.0	43.3	3.09	1.03
J093531.60+354101.0	0.4936	23.0	77.2	3.36	1.16
J104431.76+070841.0	0.6477	19.8	66.7	3.37	1.17
J224028.85−010649.8	0.1268	18.9	70.6	3.74	1.18
J152350.42+391405.2	0.6609	48.9	175.6	3.59	1.28
J130601.87+580319.9	0.4437	10.2	39.0	3.82	1.31
J092153.63+033652.6	0.3509	25.7	106.3	4.14	1.36
J083525.98+435211.3	0.5676	18.5	99.0	5.35	1.85
J131549.46+062047.8	0.3600	21.7	129.1	5.95	2.03

Figure C1. SDSS spectrum of outliers in Shen et al. (2011) sample. They have $\mathcal{R}_{\mathrm{Fe}} > 3$ and $\log{(M_{\mathrm{H}\beta,\,\mathrm{canonical}}/M_{\mathrm{H}\beta,\,\mathrm{Fe\,corrected}})} \geq 1$.

Figure C1. Continued.

This paper has been typeset from a TEX/LATEX file prepared by the author.